

**Microtexture and distribution of minerals in hydrothermal barite-silica chimney from the Franklin seamount, SW Pacific: Constraints on the mode of formation**

DURBAR RAY\*<sup>1</sup>, DALAYYA KOTA<sup>1</sup>, PRANAB DAS<sup>2</sup>, L. SURYA PRAKASH<sup>1</sup>,  
V.D. KHEDEKAR<sup>1</sup>, ANIL L. PAROPKARI<sup>1</sup>, ABHAY V. MUDHOLKAR<sup>1</sup>

<sup>1</sup>CSIR - NATIONAL INSTITUTE OF OCEANOGRAPHY, GOA-403004, INDIA

<sup>2</sup>INDIAN SCHOOL OF MINES, DHANBAD-826004, INDIA

**ABSTRACT**

Extinct hydrothermal barite-silica chimney from the Franklin Seamount of Woodlark basin was investigated for mineral distribution and geochemical composition. Six layers on either side of the orifice of a chimney showed significant disparity in colors, mineral assemblages and major element composition. Electron microscope (SEM) images reveal that peripheral wall of the chimney is composed of colloform silica suggesting incipient precipitation of silica-saturated hydrothermal fluid initiated the development of chimney-wall. Intermediate layers, between exterior wall and inner fluid-orifice, dominate with barite and sulfides. Low Sr to Ba ratios ( $\text{SrO/BaO} = 0.015\text{-}0.017$ ) indicate restricted fluid-seawater mixing causes relatively high temperature formation of intermediate layers. While, innermost layer bordering the chimney-orifice is characterized with more silica and higher Sr to Ba ratio ( $\text{SrO/BaO} = 0.023$ ), could have formed due to paragenetic shift from high temperature active phase to cooler waning stage of the chimney formation. Paragenetic shift is also responsible for the change in mineral formation mechanism that results in textural variation of barite and morphology of colloform silica developed during different growth phases of this barite-silica chimney.

Keywords: Woodlark Basin; Franklin seamount; Barite-silica chimney; mineralogy.

## 1. INTRODUCTION

The back-arc and marginal basins in southwest Pacific Ocean (e.g. Lau basin, Manus basin, Woodlark Basin, Fiji Basin, Okinawa Trough, Mariana Trough) are well known for hydrothermal activity and associated mineral deposits (Hawkins and Helu 1986; Gamo et al., 1993; Lisitzin et al., 1997; Herzig et al., 1998; Herzig and Hanington, 2000; Glasby and Notsu, 2003; Paropkari et al., 2010; Noguchi et al., 2011). Several investigations indicate that Franklin seamount in western Woodlark basin is an active submarine volcano known for present-day hydrothermal activity and related deposits (Bogdanov et al., 1997; Boyd and Scott, 2001, Laurila et al., 2012). Based on water column investigation McConachy et al. (1986); Lisitzin et al., (1991 and 1997) reported low temperature (20° - 30°C) diffused hydrothermal activity on this seamount. Detailed seafloor survey with deep-towed camera also showed the presence of hydrothermal deposits, which includes poly-metallic oxides, oxy-hydroxides, sulfate-sulfides and opaline silica (Binns et al., 1990; Binns et al., 1993; Bogdanov et al., 1997; Boyd and Scott, 2001; Hanington et al., 2005).

Binns et al. (1993) have reported that some of the chimneys or spires are made of barite and silica and discussed about their mineralogy and geochemistry. These bulk geochemical data are limited to understand the genetic history, particularly, of extinct chimneys. For better understanding about barite-silica chimney development we studied texture and zonal distribution of barite, silica and other minerals in different parts across a chimney section (from exterior wall to fluid orifice). Mostly we describe small scale variation in crystallography of barite and silica along with geochemistry to address the issues related to its genesis and development. Moreover, based on high resolution images, the formation mechanisms of minerals with different textures have been discussed. The possible temporal changes of hydrothermal fluid characteristic responsible for such mineral zoning in different part of the chimney have been described.

## 2. GEOLOGIC SETTING

Woodlark basin, located south of the Solomon Island, is a young (~ 6.0 Ma) ocean basin formed by seafloor spreading following the rifting of continental and arc lithosphere (Martinez et al., 1999). This triangular marginal basin subducts along its eastern margin beneath the New Britain trench (Fig. 1). Franklin seamount (Fig. 1) is located at the westernmost end of a neovolcanic segment of the active Woodlark spreading axis, off-shore of eastern Papua New Guinea, (Benes et al., 1994; Binns et al., 1997). This young conical seamount has well developed near circular caldera having diameter of 750 m

and depth of 100 m on its summit, rising to 2138 m from the adjacent seafloor. On the caldera-floor there are two funnel shaped depressions, which contain number of active and extinct hydrothermal chimneys (Binns et al., 1993; 1997) and filled with talus (Binns et al., 1990). Rocks from this seamount and surrounding area are mostly basaltic-andesite and contain range of pillow fragments and crust from sheet or tube flows (Binns et al., 1990; Bogdanov et al., 1997; Boyd and Scott, 2001).

### 3. SAMPLING

In 1990, during the SUPACLARK (Soviet Union–Papua New Guinea–Australia–Canada) cruises onboard *RV Akademik Mstislav Keldysh*, deep-sea submersibles (*MIR-I* and *MIR-II*) dives were undertaken to explore the hydrothermal fields in the back-arc basins in southwest Pacific Ocean. Particularly, seafloor hydrothermal activities associated with initial rifting of continental crust where the Woodlark spreading axis is propagating into Papuan margin were thoroughly explored. Among the seven *MIR* dives in the Woodlark basin, three were over Franklin seamount, end of the spreading axis. At dive station, *M-2202* (09°54.45'S and 151°49.62'E), inside the caldera of this seamount (depth = 2247m), number of barite–silica chimneys of different heights were found to rise from a mound like base (Binns et al., 1997). An extinct large barite chimney (*M-2202-IA*, 15 kg, Binns et al., 1990) partly coated with amorphous Fe-oxyhydroxides was collected by mechanical arm of submersible.

The whole chimney was sliced into several (~3.0 cm thick) sections. One section, *M-2202-IA2* (Fig 2a), second from the top of the chimney was chosen for the present study. The slice of the chimney is white in colour; however, yellowish to light grey colored bands has found surrounding a partially clogged fluid conduit. These layers with different colour appeared very similar to those found in other hydrothermal chimneys and ore deposits (Susak and Crerar, 1982; Haymon, 1983; Zlotnik-Khotkevich and Andriyanova, 1987; Herzig et al., 1988; Urabe and Kusakabe, 1990, Tivey et al., 1995; Bogdanov et al., 1997; Jianbin et al., 2007; Paropkari et al., 2010). The outer rim of the chimney is fragile and white in color but inner part is relatively dark, hard and porous in nature (Fig 2b).

### 4. METHODS

Six sub-samples correspond to the layers, L-1 to L-6 of the chimney section (*M-2202-IA2*), were made based on color variation (white to light orange colored exterior rim L-1, yellow-orange to grey layers L-2, L-3 and L-4, relatively black layer L-5 with a conduit and another light grey layer L-6) as shown in Fig. 2a. After separation, samples from each layer were thoroughly washed with Milli-Q<sup>®</sup> water and dried in a hot air oven. Several small pieces (26 nos.) from different portion of layers were

randomly sampled for microscopic investigation. The gold coated particles were scanned using a scanning electron microscope (SEM) (JEOL JSM-5410LV). Energy-dispersive X-ray Spectrometer (EDS) attached with SEM was used for qualitative chemical analysis of different minerals. Mineralogy of powdered samples from six layers was determined with an XRD, (Rigaku-PW 1710) using monochromatic Cu-K $\alpha$  radiation, over  $2\theta$  range between  $05^\circ$  and  $60^\circ$ . Mineralogical interpretation of X-ray diffractograms was carried out using Traces<sup>®</sup> software. Powdered samples of each layer were fused into borate glass-bead at high temperature ( $1180^\circ\text{C}$ ) using Lithium metaborate and Di-lithium tetraborate mixture (Spectromelt<sup>®</sup> A12, Merck). Glass-beads were analysed for major element composition with an XRF (Axios-PANalytical) at National Institute of Oceanography, India.

## 5. RESULTS

All the layers has barite and colloform silica as major mineral phases with traces of sulfides like galena, pyrite, marcasite, chalcopyrite and other sulfates (Table 1). However, SEM-image based assessment indicates that there is significant disparity in mineral abundances and textures. In particular, relative abundance of barite to colloform silica abruptly changes in between these layers. Moreover, mineral habits, and their external morphology showed discrepancies in different layers. The XRF analysis of six layers did not show much variation in barium concentration ( $\text{BaO} = 38\text{-}44\%$ , Table 1) but there was significant disparity in silica and sulfur contents ( $\text{SiO}_2 = 11\text{-}24\%$ ,  $\text{SO}_3 = 08\text{-}17\%$ , Table 1). Concentration of Sr in these layers are very low ( $\text{SrO} < 1.0\%$ ).

The outermost part of the chimney (layer L-1) consists of porous soft material containing mostly globular colloform silica [ $\text{SiO}_2, n\text{H}_2\text{O}$ ]. The silica micro-spherules ( $\sim 4\text{-}10\ \mu\text{m}$  in diameter) collectively form mat (Fig. 3a) or joined together into branched tube or fibrous (Fig. 3c) structures. Some parts of layer L-1 contain pure globular silica (Fig. 3a and 3b) and few isolated barite crystals were found within this silica matrix. This layer has maximum enrichment of Sr relative to Ba ( $\text{SrO}/\text{BaO} = 0.025$ , Table 1).

Intermediate layers (i.e, L-2, L-3 and L-4) between peripheral rim and fluid-edifice showed the presence of well developed large ( $40\text{-}80\ \mu\text{m}$ ) barite crystals coated with patches of colloform silica (Figs. 4a and 5c). The layer L-6 of another side of the edifice also dominated by large sized barite and has geochemical composition comparable to the other three intermediate layers. The layers, L-2, L-3 and L-6 are characterized with plentiful barite crystals, tabular on basal pinacoid ( $T_c$ -group, Radanovic-Guzvica, 1999), elongated in  $[001]$  direction (Figs. 4a, 4b, 7a and 7c). Some of the tubular barite crystals in L-6 are found to have grown more than  $250\ \mu\text{m}$  in length (Fig. 7d) resembling typical barites in

hydrothermal chimneys (Paytan, 2002). The surface of this porous layer, L-6 reveals numerous curved apertures (Fig. 7b), suggesting slow speed fluid flow through several flow channels in this layer. In contrast, the intermediate layer, L-4 has prismatic barite crystals elongated in the [010] direction (40-60  $\mu\text{m}$  long) ( $E_b$  group, Radanovic-Guzvica, 1999) (Figs. 5e and 5f). Besides pure barite, disseminated white patches (Fig. 4c) of sulfo-salt of barium and lead (27 wt% Ba, 32.5 wt% Pb, Fig 4d) (molar ratio of Ba:Pb=1:1) have been identified in L-2 and L-3. This is likely being the solid solution of Ba/Pb sulfate. Moreover, spherical framboid (diameter  $\sim 25 \mu\text{m}$ ) of pyrite crystals (21.0% Fe and 25.6% S, Fig 4f) having distinct layered structure (Fig. 4e) were found in L-2. Several isolated galena crystals (Fig. 5a) (49 wt% Pb and 11 wt% S, Fig. 5b) with well developed crystal facets were identified in L-4. The layer, L-6 contains rare sodium-iron-sulfate mineral, metasideronatriite,  $[\text{Na}_2\text{Fe}(\text{SO}_4)_2(\text{OH})\cdot\text{H}_2\text{O}]$ . Radiating aggregates of lath-shaped crystals of metasideronatriite (Fig. 7e) having 12-16 wt% Na, 16-19 wt% Fe and 20.5-23 wt% S were found in EDS analysis (Fig. 7f). The XRD peaks having characteristic d-spacing of  $3.67\text{\AA}$  ( $2\theta = 24.32^\circ$ ) and  $6.62\text{\AA}$  ( $2\theta = 13.38^\circ$ ) also confirms metasideronatriite in this layer. Amorphous silica is less abundant in the intermediate layers but morphology of silica globules vary in different layers. The colloform silica in L-2 and L-3 has spherical shape and looks firmly attached on barite surface (Fig 4a). While in L-4, mostly two microspheres (average diameter  $< 1.0 \mu\text{m}$ ) of colloform silica are connected with each other and develop dumbbell-like shape (Figs. 5c and 5d). Comparatively larger silica globules in L-6, are joined to one another to form chain like structure (Fig. 8a) and have dark colored (1.0-1.5  $\mu\text{m}$  thick) band around the joints (Fig. 8b). Some silica globules have small growths (Fig. 8a) on their surface.

Samples from the black colored section, L-5 surrounding the orifice, are almost devoid of barite and comprise of silica. The inner wall of the fluid conduit contains frondescent (Fig. 6c) and radiating barite (Fig. 6d) bunches which don't have well defined crystal faces. Colloform silica microspheres in L-5 (Fig. 6a) are merged with each other to form cauliflower-like assemblages. Magnified image (Fig. 6b) reveals that there are numerous openings on the surface of these silica microspheres, possibly indicates the fluid channels. Silica microspheres ( $> 10 \mu\text{m}$  in diameter) in L-5 are slightly larger than those in other sections ( $< 10 \mu\text{m}$  in diameter). The least BaO/SiO<sub>2</sub> ratio (=1.62, Table 1) and highest silica content (SiO<sub>2</sub> = 24%, Table 1) of L-5 further agree well with least abundances of barite relative to amorphous silica around the chimney orifice.

## 6. DISCUSSION

Previous investigations have shown that changes in hydrothermal fluid temperature and chemical composition develop mineral zonations in hydrothermal chimney and deposits (Haymon, 1983; Stüben et al., 1994; Tivey et al., 1995; Paropkari et al., 2010). Some of these investigations have described the growth history and related factors (Susak and Crerar, 1982; Haymon, 1983; Stüben et al., 1994; Paropkari et al., 2010) of hydrothermal deposits based on the characteristic mineral assemblages developing different colored layers. The barite-silica chimney of present investigation had white-pale yellow-brown colored layers around the fluid conduit. This layered structure has grown from several pulses of fluids (Binns et al., 1997) probably with different physiochemical conditions.

### 6.1. Relative abundances of barite, silica and sulfides: Growth history of barite-silica chimneys

The microscopic and geochemical investigation show that the outermost rim (L-1) and layer having orifice (L-5) are dominated with amorphous silica while intermediate layers (L-2, L-3, L-4 and L-6) on either sides of the conduit have abundant well crystalline barite and relatively rich in barium ( $\text{BaO/SiO}_2 = 1.9\text{--}4.0$ , Table-1). Analogous mineral distribution with filamentous and tubular silica without any barite in the outer and inner part of a barite-silica chimney wall has been reported in Kuroko hydrothermal deposits of Izu-Bonin arc (Urabe and Kusakabe, 1990). This relative mineral distribution across the wall indicates that low temperature silica rich fluids have precipitated layer, L-1 at the very early stage of chimney development. While intermediate layers (e.g. L-2, L-3, L-4 and L-6) with well crystalline barite and disseminated sulfides would have formed from fluids containing high concentration of dissolved barium (Feng and Roberts, 2011; Aloisi et al., 2004) and hydrogen sulfide ( $\text{H}_2\text{S}$ ). Relative enrichment of bulk sulfur ( $\text{SO}_3 \geq 10\%$ ) in these four intermediate sections also validates the hypothesis. Enrichment of silica in L-5 indicates precipitation of silica-rich fluid from mature chimney, before they became inactive.

Lack of sulfides and relative enrichment of colloform silica in the outermost rim indicate early initiation of low-temperature silica based structure. Presence of amorphous silica mat at the exterior rim (Figs 3a and 3d) indicates that the fluid expelled during early stage of chimney development had high concentration of dissolved silica, sufficient to maintain higher degree of super-saturation. Lisitzin et al., 1997 showed that Si concentrations ( $10.6 - 15 \mu\text{g-atom/L}$ ) in hydrothermal fluid from the Franklin Seamount is about 100 times higher than local seawater ( $0.117 \mu\text{g-atom/L}$ ). High concentration of dissolved silica in hydrothermal fluid might have originated by the interaction of seawater and basaltic-

andesite type basement rock. On mixing with cold ambient seawater, sudden decrease of fluid temperature makes the fluid oversaturated with dissolved silica, even at rates faster than crystallization, and thus forms amorphous silica indicating incipient precipitation of silica rich fluid. High Sr to Ba ratio of L-1 suggests low temperature of formation since an increase in Sr relative to Ba occurs when increased amounts of ambient seawater (source for Sr) dilute the vent fluid (Hannington and Scott, 1988; Halbatch et al., 2002). Rough surface (found as white scratches) of colloform silica microspheres (Fig. 3d) is possibly due to late stage partial dissolution of silica in contact with ambient seawater, under-saturated with respect to dissolved silica. Building of similar framework with spheroidal and fibrous silica has been also reported by Stüben et al., 1994 for barite silica chimney in “Topless Tower” of Mariana field.

Once the outer wall (of amorphous silica) of the chimney is formed, it restricted the hydrothermal fluid from mixing with the immediate ambient seawater. Thus the intermediate layers would have formed from the barium and sulfide-rich high temperature fluid. During this growth period restricted fluid-seawater mixing maintains the saturation of barium sulfate and results in large number of well crystallized barite in layers L-2, L-3, L-4 and L-6. Comparatively low Sr to Ba ratios ( $\text{SrO}/\text{BaO} = 0.015 - 0.022$ , Table 1) of these intermediate sections also indicates limited influence of ambient seawater and thus higher temperature of formation. The gradual change in Sr to Ba ratios among these intermediate layers (e.g.  $L-4 < L-3 < L-2$ , Table 1) suggests that there was temperature gradient between edifice to outer wall. Some parts of L-2 show extensive crystallization of smaller platy barite (Fig. 4b) indicating presence of more number of crystal nuclei. Such dense patch of nuclei formation commonly occurred due to sudden drop in temperature of super-saturated fluid (Qi et al., 2000). Experimental results on growth mechanism of barite crystal by Pina et al. (1998) conclude that addition of more supersaturated solution can cause higher nucleation density. Occurrence of disseminated sulfide minerals (e.g. galena, pyrite, marcasite etc.) in these layers (Figs 4e and 5a) suggests the presence of  $\text{H}_2\text{S}$  in end member hydrothermal fluid. However, earlier hydrological study showed that low temperature, slightly acidic ( $\text{pH} = 6.26$ ) hydrothermal fluid of Franklin seamount has no measurable dissolved  $\text{H}_2\text{S}$  (Lisitzin et al., 1997). Therefore, these isolated framboidal pyrite and other sulfide crystals might form due to episodic fluxes of metal-enriched,  $\text{H}_2\text{S}$  bearing reducing hydrothermal fluid. The Ba/Pb-sulfate solid solution along with pure barite in these intermediate layers suggests that the ascending vent fluid was rich in dissolved Pb. It has been found that hydrothermal fluid emerging at station *M-2202* inside the caldera of the Franklin seamount has higher lead content ( $\text{Pb} = 1.2 \text{ nmoles/L}$ ; Lisitzin et al., 1997).

Scott and Binns, (1995) also noted enrichment of lead in lava of Franklin seamount and thus confirmed that the sub-seafloor magma is the source of dissolved lead in fluid. Similar observations have been reported in Tamagawa hot spring in Japan (Sasaki and Watanuki, 1983).

In the late stage of paragenetic sequence, fluid flow and temperature gradually drops and more silica precipitates from relatively cooler fluid having higher oxygen fugacity and neutral to alkaline pH. In mature chimney, low rate of fluid flow and rapid accumulation of silica near the chimney orifice slowly chokes up its opening as found in layer L-5. Traces of sulfide minerals were found in L-5 but considerable amount of metasideronatriite, produced through sulfides-oxidation, was present around the conduit (particularly in layers L-6 and L-5). Fluid emitted in the late stage of paragenetic shift cause's alteration of sulfides (e.g. pyrite, chalcopyrite, pyrrhotite, sphalerite) precipitated from high temperature-low pH fluid at the initial stage (Duckworth et. al., 1994). Occurrence of metasideronatriite,  $[\text{Na}_2\text{Fe}(\text{SO}_4)_2(\text{OH})\cdot\text{H}_2\text{O}]$ , usually formed by alteration of sideronatriite  $[\text{Na}_2\text{Fe}(\text{SO}_4)_2(\text{OH})\cdot 3\text{H}_2\text{O}]$ , an oxidative product of pyrite  $[\text{FeS}_2]$  or pyrrhotite  $[\text{Fe}_{(1-x)}\text{S}]$  suggest that there was adequate interaction with seawater, as the chimney became extinct. Higher Sr to Ba ratio ( $\text{SrO}/\text{BaO} = 0.023$ ) in L-5 also support the contribution of seawater during waning phase of chimney development.

The mineralogical and geochemical provinces across this chimney wall broadly display its three distinct mineral zones and indicate three major phases of chimney development. Growth phases mainly include 1) early development of silica-rich wall, 2) thickening of the wall due to high temperature barite-sulfide-silica mineralization and 3) late stage silicification as the chimney cools down. Schematic illustration in Fig 9 is presenting the possible step-wise minerals development along with the growth of chimney. A similar growth history of silica-rich chimney within the median rift valley of the Mariana Trough in SW-Pacific was suggested by Stüben et al., (1994).

## **6.2. Variation in microtexture of barite crystals: Changes in physiochemical condition of hydrothermal fluid**

The crystallographic features of barite are different in layers across the chimney section. Dendritic frondescent barites (Figs 6c and 6d) were found around the chimney edifice (L-5) but well crystalline orthorhombic barites (Figs 4b and 5f) developed in the intermediate layers, L-2, L-3, L-4 and L-6. Morphologies of barite crystal in different layers suggest changes in physiochemical condition of depositional environment and can provide information regarding their formation (Paytan et. al., 2002; Feng and Roberts, 2011). Experimental results showed that morphology of barite crystals changes with



increase in concentration product,  $(m_{Ba^{2+}})(m_{SO_4^{2-}})$  and thus with saturation index,  $[SI = (m_{Ba^{2+}})(m_{SO_4^{2-}})/K_{sp}$ , where  $K_{sp}$  is solubility product] (Nielsen, 1958) of the solution. Dendritic barites normally precipitate from a solution having high degree of saturation with respect to barium and sulfate ions following bulk diffusion mechanism, while surface reaction mechanism develops crystalline barite in low saturated solution (Shikazono, 1994). Therefore, during high temperature active phase of the chimney, polynuclear crystals likely precipitated from fluid of low saturation and developed abundant well formed crystalline barites in intermediate layers. In contrast, at the waning phase, cooling of the chimney is expected to facilitate the emerging fluid to attain higher level of saturation and thus dendritic barites grow around the chimney edifice.

Moreover, the rectangular platy barites (Figs 4a and 4b) of intermediate layers, L-2 and L-3 differ from elongated prismatic type barite crystals (Fig 5f) in layer L-4. The large prismatic barite crystals, elongated in [010] direction usually have higher structural density than smaller platy [001] barite (Radanovic-Guzvica, 1999). Two habits of barite in these layers could be the result of either physiochemical changes of fluid during separate pulses of hydrothermal emission or late stage alteration and re-crystallization of platy barites into prismatic type in higher temperature zones. The formation of variety of barites in these layers is not clear. However, abundant larger prismatic barites nearer to fluid conduit and more platy barites in cooler outward side of the chimney wall possibly indicates the crystallographic change due to temperature gradient developed by conductive cooling across the chimney-wall. Shikazono (1994) reported coarse-grained polyhedral barite in the inner part of sulfate-sulfide chimneys from Kuroko and Mariana basins. The least abundance of Sr relative to Ba ( $SrO/BaO = 0.015$ ) in layer L-4 suggests minimum mixing of seawater with the hydrothermal fluid and precipitation occurred at highest temperature.

### **6.3. Textural variation of colloform silica: Mode of silica precipitation from the hydrothermal fluid**

It has been found that the morphology of silica micro-spherules and their aggregates significantly varies in different layers of the chimney. Broadly all these morphological features can be classified into two major groups. The type-I aggregate have closely spaced microspherules adhere or attached with each other (globules, Figs 3a,d or cauliflower shaped, Fig 6a) while type -II aggregate have microspherules of different size and connecting through distinct separating channel or band (chains, Fig 8a or dumbbell shaped, Fig 5d). Type-I silica was mostly found in exterior L-1 and near the conduit, L-

5. These type aggregate must have formed together due to instantaneous precipitation of silica saturated fluid in contact with ambient seawater. In contrast, type-II silica within the intermediate layers, L-2, L-3, L-4 and L-6 are likely formed at slower rate from more viscous fluid at higher temperature. The silica microspheres precipitated from viscous fluid contains residual melts inside and the gas pressure of entrapped melts helped to blow out new adjacent microspheres. The small growths shown in Fig 8a confirms that silica chains developed as new spheres grow on existing spheres. So it can be hypothesized that the growth of new spheres was likely started through partial melting of parent spheres wall in contact with hot volatile rich fluid inside. Thus fluid-flow channels connect the microspheres into chains, tube or dumbbell shaped siliceous structures. A circular fluid channel entrance can be seen as a part of a broken sphere in Fig. 8c. The circular bands around the joint of two spheres (Fig. 8b) represent the flow channel between the microspheres, developed during trapped fluid-sphere wall interaction. In some instance closely spaced growths of these spheres developed tube or rod like structures as seen in Fig. 8d, similar to pure chert microspheres reported by Halbach et al. (2002) in hydrothermal deposits.

## 7. CONCLUSION

Six layers from wall to orifice of a hydrothermal barite chimney section had analogous bulk composition of barite and colloform silica; however their abundance and texture varies considerably. Relative abundances and textural variety of silica and barite crystals marking three distinct mineral zones across the chimney section suggest three major phases of chimney development. In early stage growth of chimney starts with silicious wall formation and then it filled inward with barite-silica-sulfides and finally silicified during extinction.

Alteration of temperature and composition of hydrothermal fluid are mainly responsible for the change in mineral assemblages and habits during three growth phases of the chimney. Initially silica precipitated as aggregate of microspheres from low temperature silica-rich fluid. Once the silica wall was in place, restricted mixing with seawater causes mineral formation at higher temperature and thus tabular or prismatic barites and dumbbell or chain like silica structures were developed. In late stage as the chimney cools down dendritic barite crystals and more silica microspheres were developed from the fluid supersaturated with barium and silica.

Acknowledgements: The authors are thankful to the Director, National Institute of Oceanography, Goa for his permission to publish the work. Dr. Paropkari is grateful to Prof. Alexander. P. Lisitzin for

inviting him to participate in the 21<sup>st</sup> cruise of *R.V. Akademik Mstislav Keldysh* and providing the samples to undertake the investigations. Our appreciation goes to Mr. Girish Prabhu for XRD analysis and N. R. Moraes Ceasar for XRF analysis. Thanks to Mr S. G. Akerker for making sketch of the model. Authors are thankful to the editor and anonymous reviewer for their valuable comments. This is NIO contribution no. -----.

## REFERENCES:

- Aloisi, G., Wallmann, K., Bollwerk, S.M., Derkachev, A., Bohrmann, G., Suess, E., 2004. The effect of dissolved barium on biogeochemical processes at cold seeps. *Geochimica et Cosmochimica Acta* **68**, 1735–1748.
- Benes, V., Scott, S.D., and Binns, R.A., 1994. Tectonics of rift propagation into a continental margin: Western Woodlark basin, Papua New Guinea. *Journal of Geophysical Research* **99**, 4439-4455.
- Binns, R.A., Parr, J.M., Gemmell, J.B., Whitford, D.J. and Dean, J.A., 1997. Precious metals in barite-silica chimneys from Franklin seamount, Woodlark basin, Papua New Guinea. *Marine Geology* **142**, 119-141.
- Binns, R.A., Scott, A.D., Bogdanov, Y.A., Lisitzin, A.P., Gordeev, V.V., Gurvich, E.G., Finlayson, E.J., Boyd, T., Dotter, I.E., Wheller, G.E. and Muravyev, K.G., 1993. Hydrothermal oxide and gold-rich sulfate deposits of Franklin seamount, western Woodlark basin, Papua New Guinea. *Economic Geology* **88**, 2122-2153.
- Binns, R.A., Scott, A.D., Wheller G.E., Benes V., 1990. Report on the Supaclark Cruise, Woodlark basin, Papua New Guinea, 08-28 April, 1990, RV Akademik Keldysh.
- Bogdanov, Y.A., Lisitzin, A.P., Binns, R.A., Gorshkov, A.I., Gurvich, E.G., Dritz, V.A., Dubinina, G.A., Bogdanova, O.Y., Sivkov, A.V. and Kuptsov, V.M., 1997. Low temperature hydrothermal deposits of Franklin seamount, Woodlark basin, Papua New Guinea. *Marine Geology* **142**, 99-117.
- Boyd, T.D., and Scott, S.D., 2001. Microbial and hydrothermal aspects of ferric oxyhydroxides and ferrosic hydroxides: the example of Franklin Seamount, western Woodlark Basin, Papua New Guinea. *Geochemical Transactions* doi: 10.1039/b105277m.
- Duckworth, R.C., Fallick, A.E. and Rickard, D., 1994. Minerology and sulfur isotope composition of the middle valley massive sulfide deposit, northern Juan de Fuca ridge. In: "Proceedings of the ocean drilling program, scientific results", Mottl, M.J., Davis, E.E., Fisher, A.T., Slack, J.F. (eds.) **139**, 373-385.
- Feng, D., and Roberts H.H., 2011. Geochemical characteristics of the barite deposits at cold seeps from the northern Gulf of Mexico continental slope. *Earth and Planetary Science Letters* **309**, 89-99.
- Gamo, T., Sakai, H., Ishibashi, J., Nakayama, E., Isshiki, H., Matsuura, H., Shitashima, K., Takeuchi, K. and Ohta, S., 1993. Hydrothermal plumes in the eastern Manus basin, Bismarck Sea: CH<sub>4</sub>, Mn, Al and pH anomalies. *Deep Sea Research (I)* **40**, 2335-2349.

- Glasby, G.P. and Notsu, K., 2003. Submarine hydrothermal mineralization in the Okinawa Trough, SW of Japan: an overview. *Ore Geology Reviews* **23**, 299–339.
- Halbach, M., Halbach, P., and Luders, V., 2002. Sulfide-impregnated and pure silica precipitates of hydrothermal origin from the central Indian Ocean. *Chemical Geology* **182**, 357–375.
- Hannington, M.D., and Scott, S.D., 1988. Mineralogy and geochemistry of a hydrothermal silica–sulfide–sulfate spire in the caldera of axial seamount, Juan de Fuca Ridge. *Canadian Mineralogist* **26**, 603–625.
- Hawkins, J., and Helu, S., 1986. Polymetallic sulfide deposit from “black smoker” chimney: lau basin. *Eos-Transactions, AGU* **67**, 378.
- Haymon, R.M., 1983. Growth history of hydrothermal black smoker chimney. *Nature* **301**, 695–698.
- Herzig, P.M., Becker, K.P., Stoffers, P., Bäcker, H., and Blum, N., 1988, Hydrothermal silica chimney fields in the Galapagos Spreading Center at 86°W. *Earth and Planetary Science Letters* **89**, 261–272.
- Herzig, P.M., and Hannington, M.D., 2000, Polymetallic massive sulfide and gold mineralization at mid-ocean ridges and in subduction related environments. In: “Handbook of marine mineral deposits”, Cronan D.S. (ed.), CRC Press, London 347–368.
- Jianbin, Z., Zhimin, C., and Wei, A., 2007. Mineral components, textures and forming conditions of hydrothermal chimney on the east pacific rise at 9°–10° N. *Journal of China University of Geosciences* **18**, 128–134.
- Laurila, T. E., Petersen, S., Devey, C. W., Baker, E. T., Augustin, N., Hannington, M.D., 2012. Tectonic and magmatic controls on hydrothermal activity in the Woodlark Basin, *Geochemistry Geophysics Geosystem*, **13**, Q09006, doi:10.1029/2012GC004247.
- Lisitzin, A.P., Binns, R., Bogdanov, Y., Scott, S., Zonenshayn, I., Gordeyev, V., Gurvich, Y., Murav’ev, K. and Serova, V., 1991. Active hydrothermal activity at Franklin seamount western Woodlark Sea (Papua New Guinea). *International Geology Review* **33**, 914–929.
- Lisitzin, A.P., Lukashin, V.N., Gordeev, V.V., McConachy, T.F., Scott, S.D. and Shevchenko, V.P., 1997. Hydrological and geochemical anomalies associated with hydrothermal activity in SW Pacific marginal and back-arc basins. *Marine Geology* **142**, 7–45.
- Martinez, F., Taylor, B., Goodliffe, A., 1999. Contrasting styles of seafloor spreading in the Woodlark Basin: Indications of rift-induced secondary mantle convection. *Journal of Geophysical Research* **104**, (B6), 12909–12926.
- McConachy, T.F., Whitford, D.J., Scott, S.D., 1986. Particulate matter concentration in western Woodlark Basin. *Eos. Tras., AGU*, **67**, 1028.
- Nielsen, A.E., 1958. The kinetics of crystal growth in barium sulfate precipitation. *Acta Chemica Scandinavica* **12**, 951–958.
- Noguchi, T., Shinjo, R., Ito M., Takada, J., Oomori, T., 2011. Barite geochemistry from hydrothermal chimneys of the Okinawa Trough: insight into chimney formation and fluid/sediment interaction. *Journal of Mineralogical and Petrological Sciences* **106**, 26–35.

- Paropkari, A.L., Ray, D., Balaram, V., Surya Prakash, I., Mirza, I.H., Satyanarayana, M., Gnaneshwar Rao, T. and Kaisary, S., 2010. Formation of hydrothermal deposits at Kings Triple Junction, northern Lau back-arc basin, SW Pacific: The geochemical perspectives. *Journal of Asian Earth Sciences* **38**, 121-130.
- Paytan, A., Mearon, S., Cobb, K. and Kastner, M. 2002. Origin of marine barite deposits: Sr and S isotope characterization. *Geology*, **30**, 747-750.
- Pina, C.M., Becker, U., Risthaus, P., Bosbach, D., and Putnis, A., 1998. Molecular-scale mechanisms of crystal growth in barite. *Nature* **395**, 483-486.
- Qi, L., Cölfen, H., and Antonietti, M., 2000. Control of barite morphology by double-hydrophilic block copolymers. *Chemistry of Materials* **12**, 2392-2403.
- Radanovic-Guzvica, B., 1999. The average structural density of barite crystals of different habit types. *Geologia Croatica* **52**, 59-65.
- Sasaki, N., and Watanuki, K., 1983. Variation in chemical composition of naturally occurring lead bearing barite (hokutolite) having crystallized since 1953 at Tamagawa hot spring. *Mineralogical Journal* **11**, 297-302.
- Scott, S.D., and Binns, R.A., 1995. Hydrothermal processes and contrasting styles of mineralization in the western woodlark and eastern manus basins of the western Pacific. In: "Hydrothermal vents and processes". Parson, I.M., Walkar, C.I., Dixon, D.R. (eds.), Geological society, London, Special publications. **87**, 191-205.
- Shikazono, N., 1994. Precipitation mechanisms of barite in sulfate-sulfide deposits in back-arc basins. *Geochimica et Cosmochimica Acta* **58**, 2203-2213.
- Smith, W.H.F., 1993. On the accuracy of digital bathymetric data. *Journal of Geophysical Research – Solid Earth* **98** (B6), 9591 – 9603.
- Stüben, D., Taibi, N.E., Mcmurtry, G.M., Scholten, J., Stoffers, P., and Zhang, D., 1994. Growth history of a hydrothermal silica chimney from the Mariana back-arc spreading center (southwest Pacific, 18°13'N). *Chemical Geology* **113**, 273-296.
- Susak, N.J., and Crerar, D.A., 1982. Factors controlling mineral zoning in hydrothermal ore deposits. *Economic Geology* **77**, 476-482.
- Tivey, M.K., Humphris, S.E., Thompson, G., hannington, M.D. and Rona, P.A. 1995. Deducing patterns of fluid flow and mixing within the tag active hydrothermal mound using mineralogical and geochemical data. *Journal of Geophysical Research* **100**, 12527–12555.
- Urabe, T., and Kusakabe, M., 1990. Barite-silica chimneys from the Sumisu rift, Izu-Bonin arc: possible analog to hematitic chert associated with Kuroko deposits. *Earth and Planetary Science Letters* **100**, 283-290.
- Zlotnik-Khotkevich, A., and Andriyanova, N., 1987. Origin of mineral zoning of sulfide ores in massive sulfide deposits. *International Geology Review* **29**, 1065-1072.

## Figure captions:

**Figure 1** Map showing the location of the Franklin Seamount (Red star) and geophysical setting around the Woodlark Basin in SW Pacific Ocean. Bathymetric data is obtained from Smith (1993).

**Figure 2** Barite-silica chimney from Franklin seamount, southwest Pacific. **a** Cross-sectional view of the chimney. Markings show the boundaries of six sub-samples (L-1 to L-6) used for the present study. **b** Microscopic view of inner part of chimney show porous nature of the wall.

**Figure 3** SEM-EDS results of outermost rim of the chimney section, L-1. **a** Colloform silica forming mat. **b** Presence of only silicon and oxygen peaks in EDS analysis of colloform silica reflecting its high purity **c** Branched filaments of colloform silica **d** Eroded surface of silica microspheres.

**Figure 4** SEM-EDS results of intermediate layers, L-2 and L-3. **a** Colloform silica spheres stucked on tabular barite crystals elongated in [001] direction. **b** Dense nucleation of barite crystals. **c** Massive Ba/Pb-sulfate solid solution (white patches, indicated with black arrows) associated with barite. **d** EDS pattern of Ba/Pb-sulfate solid solution. **e** Isolated sphere of framboidal pyrite crystal. **f** EDS results of framboidal pyrite.

**Figure 5** SEM-EDS results of layer L-4. **a** Isolated octahedral galena crystal on silica mat. **b** EDS results of galena crystal. **c** Disseminated dumbbell shaped amorphous silica microspheres attached on barite crystal. **d** Magnified image of dumbbell shaped silica. **e** and **f** Prismatic barite crystals elongated in [010] direction..

**Figure 6** Selective SEM images of silica and barite crystals from layer L-5. **a** Cauliflower shaped colloform silica aggregates. **b** Magnified image of silica aggregate reveals rough surface of the microspheres. **c** Frondescent and **d** Radiated type dendritic barite deposits inside the fluid conduit.

**Figure 7** SEM-EDS results of layer L-6. **a** Bulbous colloform silica deposits on barite. **b** Fluid flow openings (indicated with white arrow) on barite surface. **c** and **d** Tabular barite crystals with distinct crystal faces. **e** Cluster of lath-shaped metasideronatrite crystals. **f** EDS results showing composition of metasideronatrite.

**Figure 8** SEM-images of microspheres of colloform silica from the section L-6. **a** Chain of microspheres with a small growth of new sphere (as shown with arrow). **b** Typical band (showed with arrow) at the joints of microspheres. **c** Broken part at the joint of microspheres indicating fluid flow channel (white arrow). **d** Merged silica spheres forming tube-like structures.

**Figure 9** Schematic presentations of idealized vertical section of hydrothermal barite-silica chimney/spire during three major growth phases (modified after Haymon, 1983). **a** Initial chimney growth starts with the development of silica walls. **b** Inside the wall restricted mixing of seawater and hydrothermal fluid develops more barite and sulfides surrounding the central conduit. **c** Drop in fluid flow and more mixing with seawater causes precipitation of colloform silica, which block the fluid channel(s) over the period of time. The section of chimney used for present study.

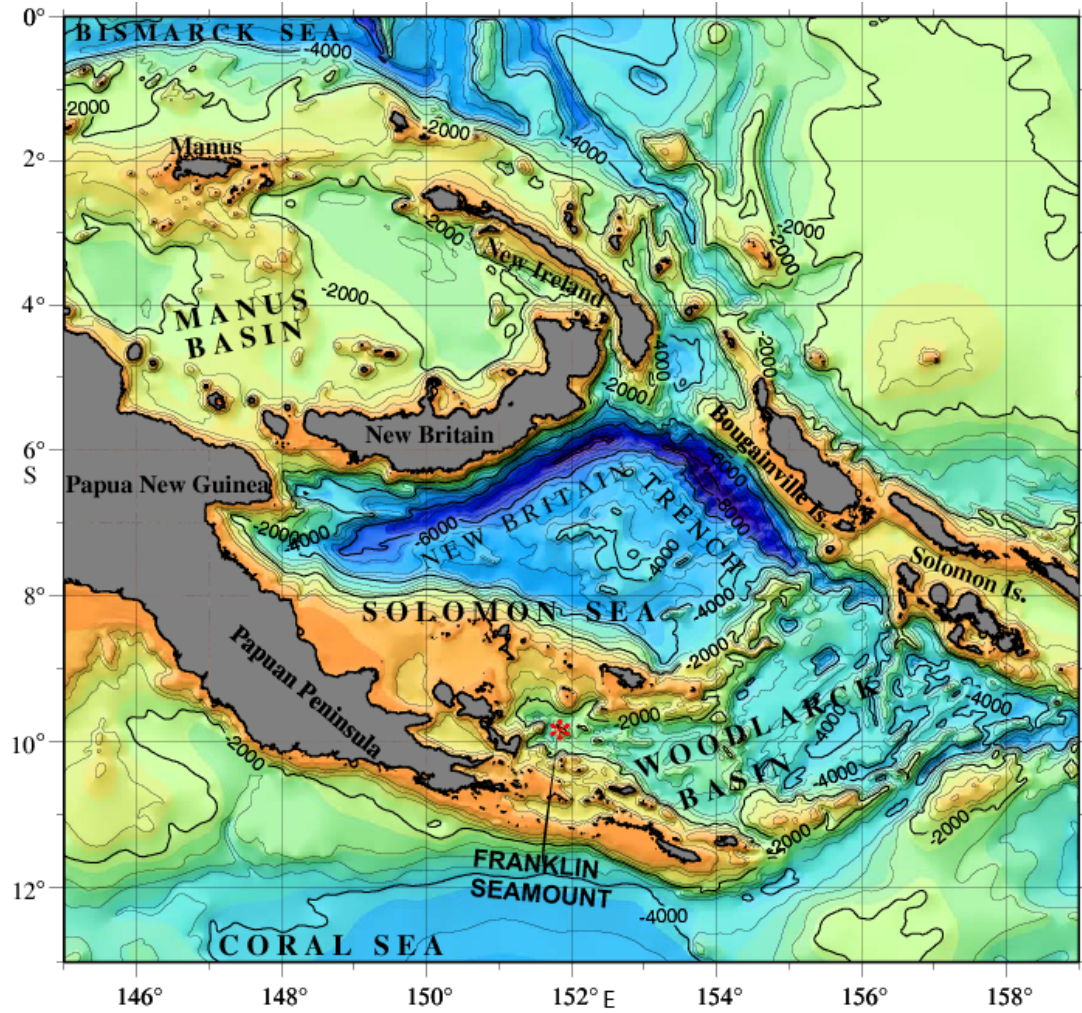


Figure 1

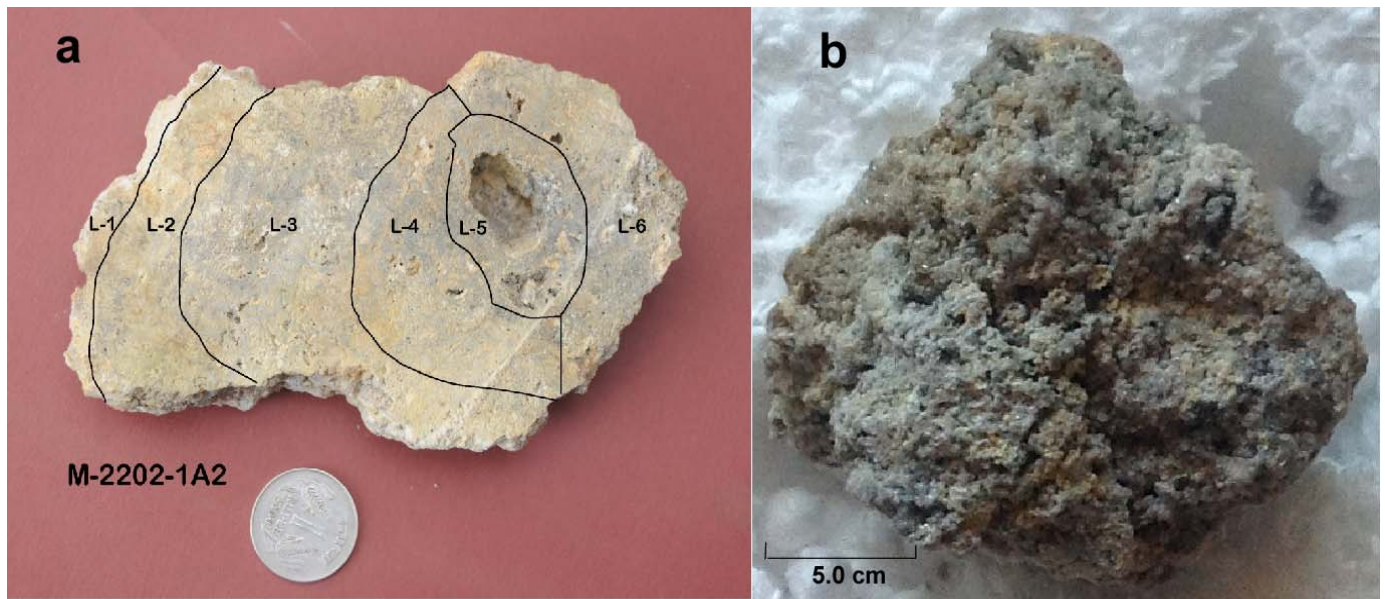


Figure 2

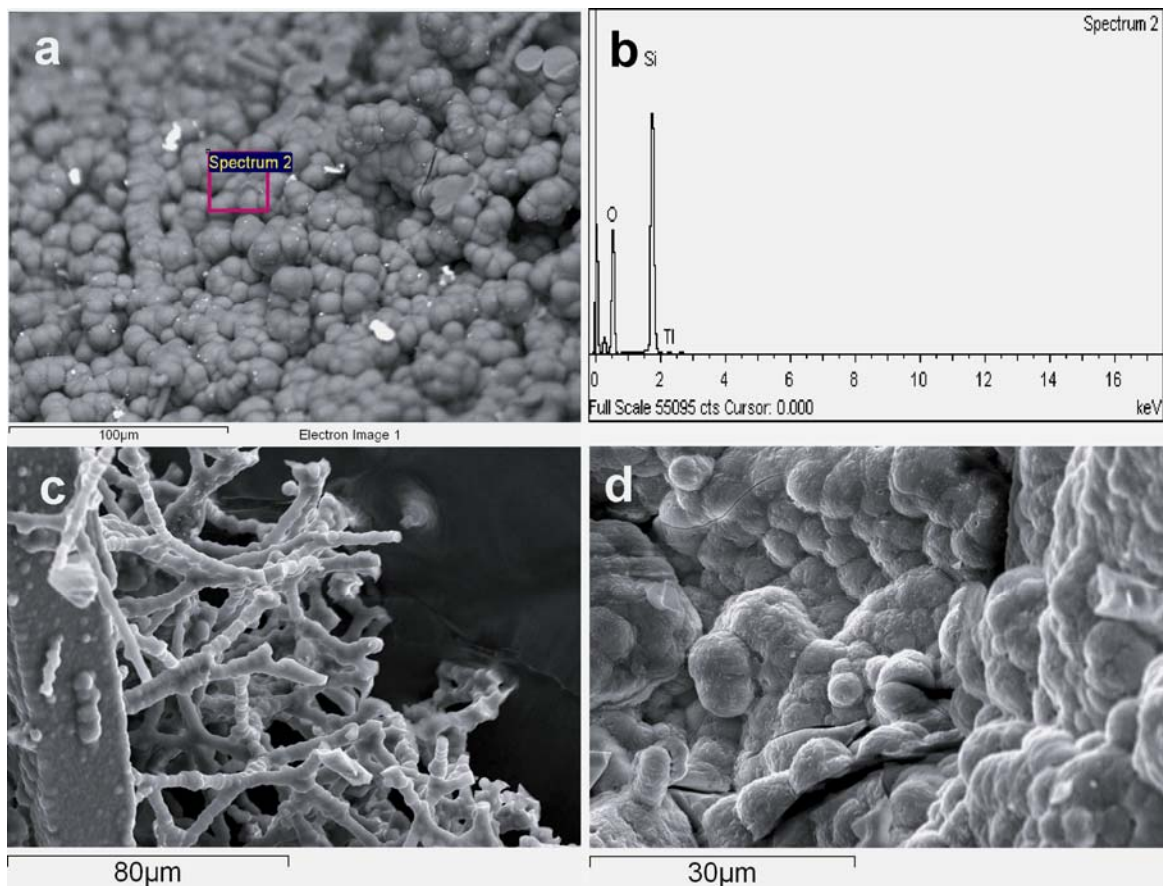
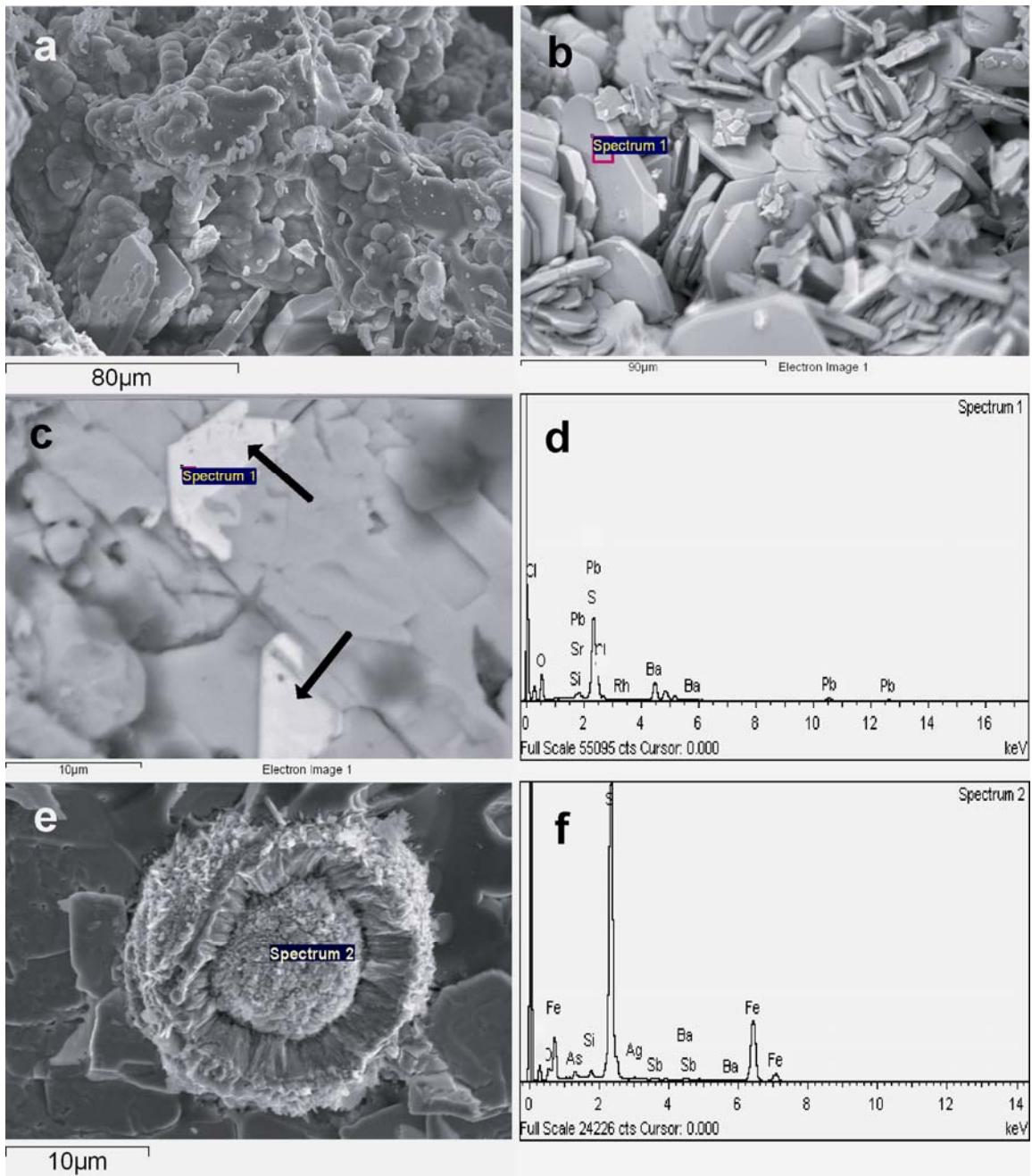


Figure 3





**Figure 4**

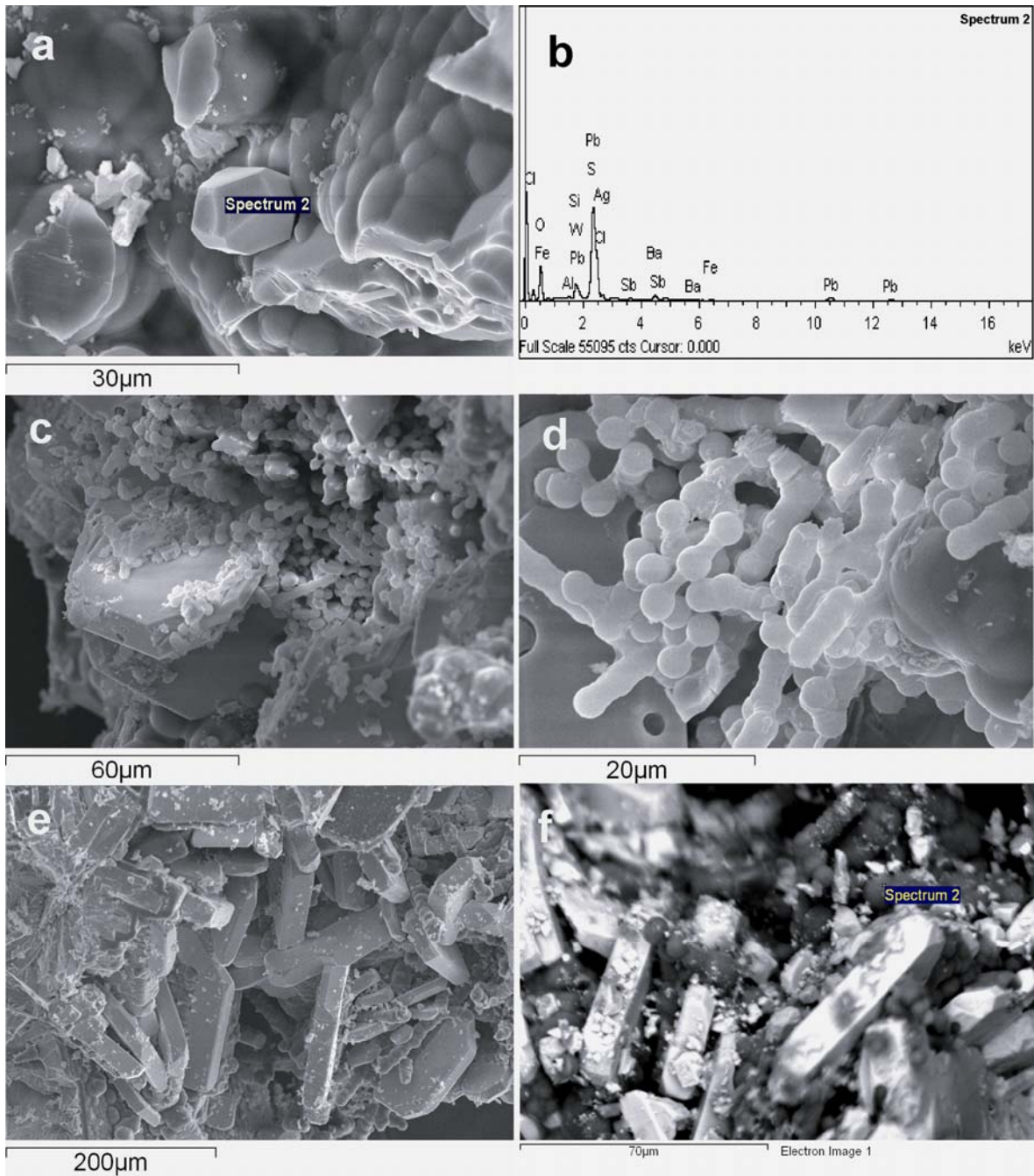
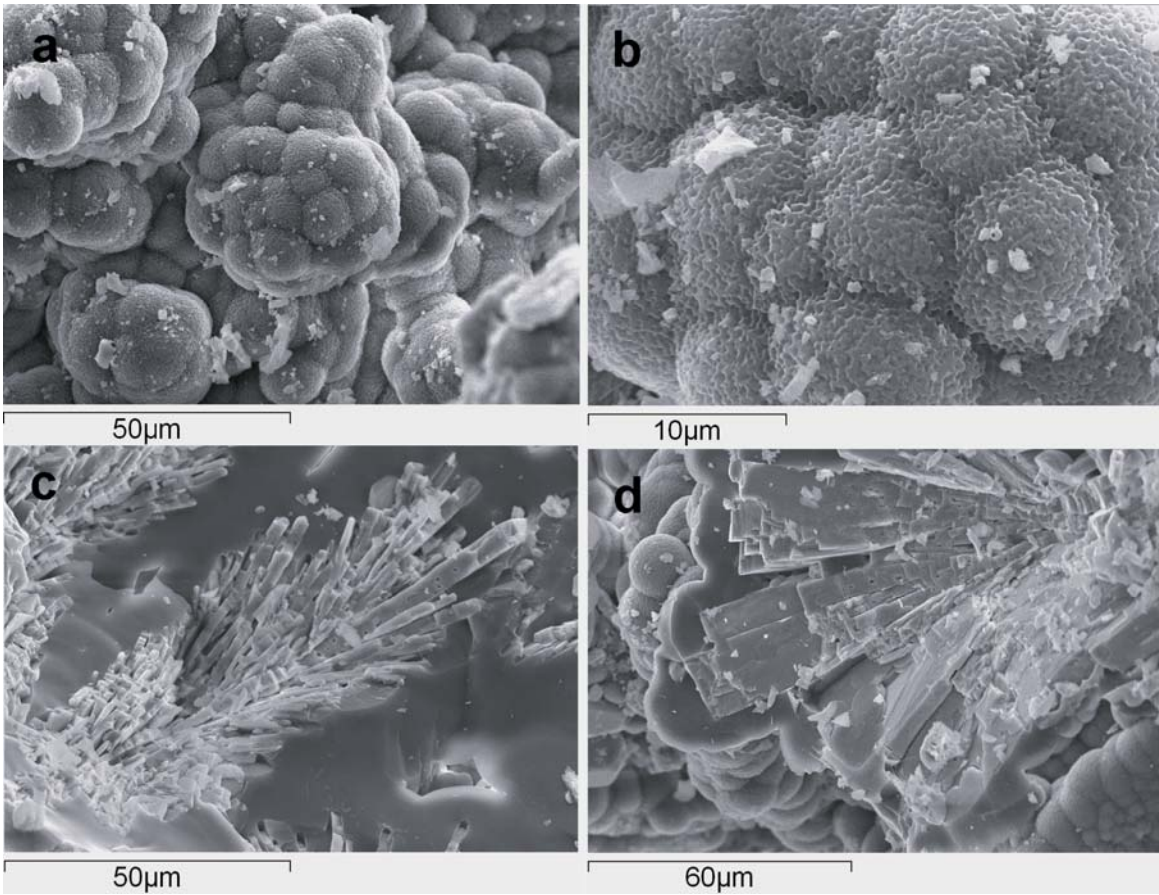


Figure 5



**Figure 6**

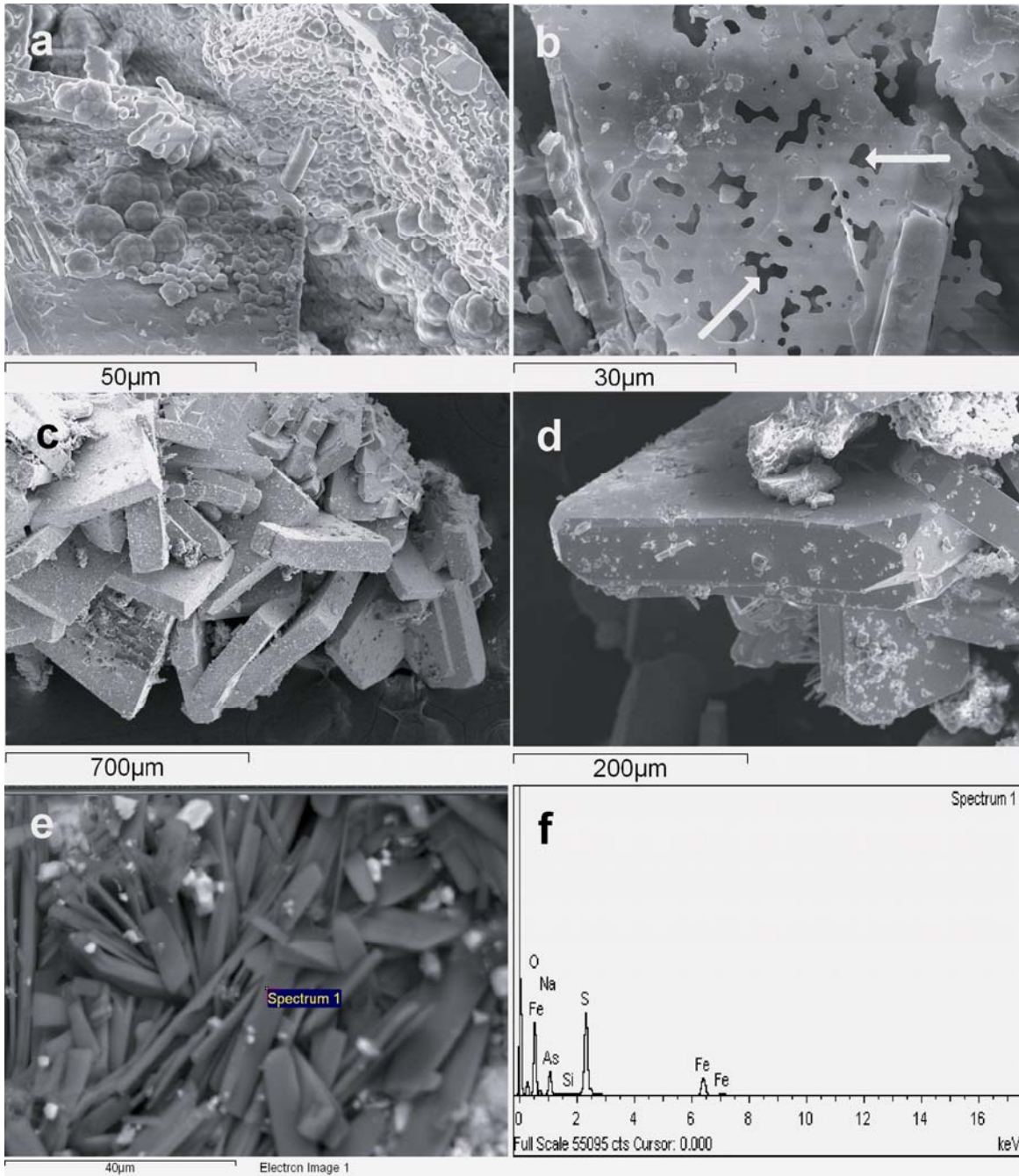
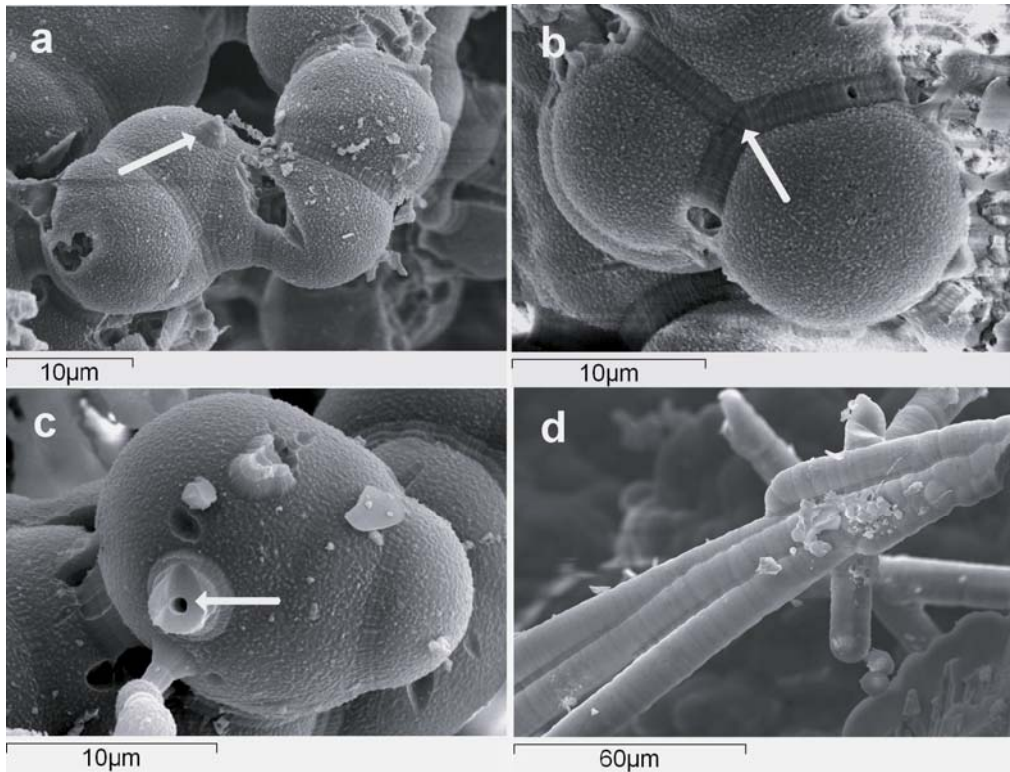
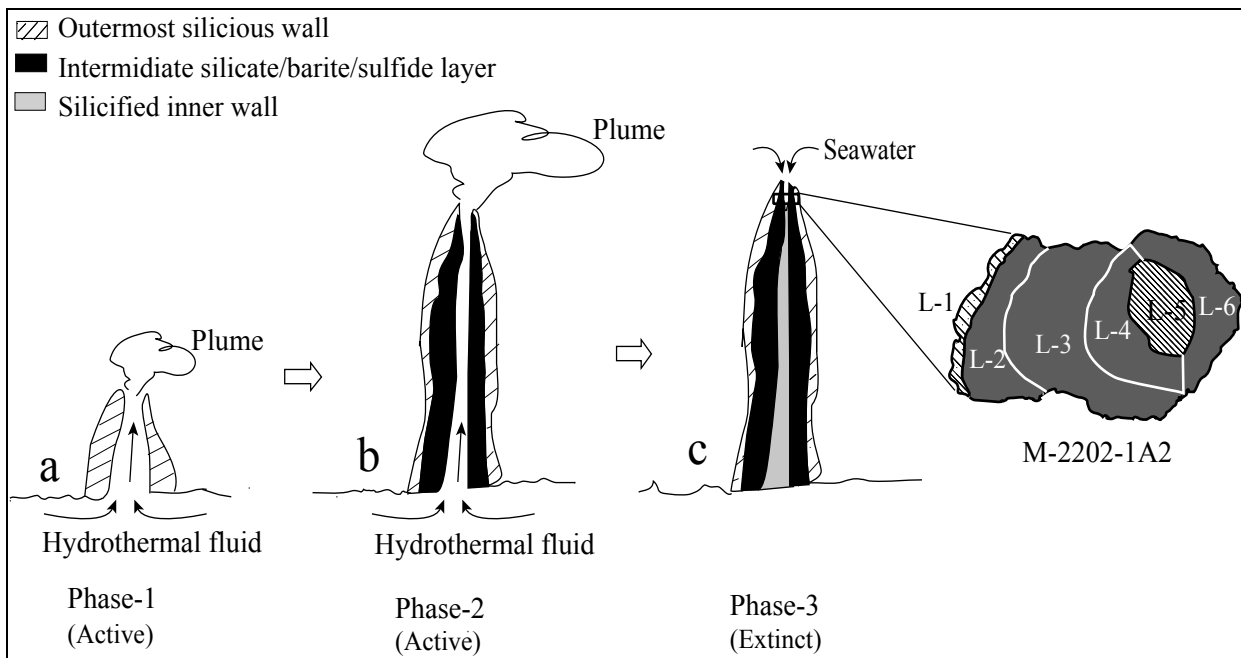


Figure 7



**Figure 8**



**Figure 9**

**Table 1:** Mineralogy and major element composition of the six layers across a section of the barite-silica chimney, *M-2202-1A* collected from the Franklin seamount, Woodlark basin, SW Pacific Ocean.

Chimney layers	Thicker wall of the chimney section				Conduit	Thin wall
	Exterior rim of the wall (L-1)	Intermediate part of the wall between outermost rim and inner conduit (L-2) (L-3) (L-4)			Layer with conduit (L-5)	Layer with thin wall (L-6)
Major minerals	col-si, br	br,	br,	br,	br, col-si,	col-si, br
Other trace minerals	---	col-si ga, py	col-si ga, py	py, cp, mr, st, anh, col-si	msn, py, anh	msn
SiO <sub>2</sub> (%)	23	14	18	20	24	12
Al <sub>2</sub> O <sub>3</sub> (%)	0.3	0.2	0.2	0.3	0.2	0.3
Fe <sub>2</sub> O <sub>3</sub> (%)	18	18	19	18	18	19
MnO (%)	nd	0.8	0.7	nd	0.7	0.7
Cr <sub>2</sub> O <sub>3</sub> (%)	7.0	7.0	7.0	7.0	7.0	8.0
NiO (%)	0.7	0.8	0.8	0.8	0.8	0.8
BaO (%)	40	40	42	38	39	44
SrO (%)	1.0	0.7	0.7	0.6	0.9	1.0
CaO (%)	0.2	0.2	0.2	0.1	0.1	0.2
Na <sub>2</sub> O (%)	0.6	0.7	0.7	0.6	0.6	0.7
SO <sub>3</sub> (%)	8.0	17	11	13	9.0	11
Total	98.9	99.4	100.3	98.4	100.3	97.7
BaO/SiO <sub>2</sub>	1.74	2.86	2.33	1.9	1.62	3.66
SrO/BaO	0.025	0.017	0.017	0.016	0.023	0.022

*Note:* anh = Anhydrite; br = Barite; col-si = Colloform silica; cp = Chalcopyrite; ga = Galena; mr = Marcasite; msn = Metasideronatrinite; py = Pyrite; st = Strontianite; nd = Not detectable.